Mon. Not. R. Astron. Soc. **000**, 1–?? (2008) Printed 5 June 2009 (MN LATEX style file v2.2)

Weather at Sierra Negra: 7.3-year statistics and a new method to estimate the temporal fraction of cloud cover

E. Carrasco,[1⋆] A. Carramiñana,[1] R. Avila,[2] C. Gutiérrez,[1] J. L. Avilés,[1,2] J. Reyes,[1] J. Meza[1] and O. Yam[3]
[1] *Instituto Nacional de Astrofísica, Óptica y Electrónica, Luis Enrique Erro 1, Tonantzintla, Puebla, C.P. 72840, México*
[2] *Centro de Radioastronomía y Astrofísica, UNAM, Apartado Postal 3-72, Morelia, Michoacán, C.P. 58089, México*
[3] *Universidad de Quintana Roo, Boulevard Bahía S/N, Chetumal 77019, Quintana Roo, México*

ABSTRACT
Sierra Negra, one of the highest peaks in central Mexico, is the site of the Large Millimeter Telescope. We describe the first results of a comprehensive analysis of the weather data measured in situ from October 2000 to February 2008 to be used as a reference for future activity in the site. We compare the data from two different stations at the summit considering the accuracy of both instruments. We analysed the diurnal, seasonal and annual cycles for all the parameters. The thermal stability is remarkably good, crucial for a good performance of the telescopes. From the solar radiation data we developed a new method to estimate the fraction of time when the sky is clear of clouds. We show that our measurements are consistent with a warm standard atmosphere model. The conditions at the site are benign and stable given its altitude, showing that Sierra Negra is a extremely good site for millimeter and high energy observations.

Key words: site testing — atmospheric effects

1 INTRODUCTION

High altitude astronomical sites are a scarce commodity with increasing demand. A thin atmosphere can make a substantial difference in the performance of scientific research instruments like millimeter-wave telescopes or water Čerenkov observatories. In our planet reaching above 4000 metres involves confronting highly adverse meteorological conditions. Sierra Negra, the site of The Large Millimeter Telescope/El Gran Telescopio Milimétrico (LMT) is exceptional in being one of the highests astronomical sites available with endurable weather conditions. The LMT site combines high altitude (4580 m) and low atmospheric water content. The water vapor opacity has been monitored since 1997 with radiometers working at 225 GHz showing that the zenith transmission at the site is better than 0.89 at 1 mm during 7 months of the year and better than 0.80 at 850 microns during 3 months of the year (Hughes 2008). There is no telescope as massive as the LMT above 4500 metres anywhere else and one can barely expect to operate at that altitude with temperatures above freezing. The development of the LMT site led to the interest and development of other scientific facilities benefiting from the high altitude conditions and sharing the same basic infrastructure. In July 2007 the base of Sierra Negra was selected as the site for the High Altitude Water Čerenkov (HAWC) gamma-ray observatory, an instrument whose performance depends critically on its 4100 m altitude location.

2 THE SIERRA NEGRA SITE

Sierra Negra, also known as Tliltepetl, is a 4580 meter volcano inside the Parque Nacional Pico de Orizaba, a national park named after the highest mountain of Mexico. With an altitude of 5610 m[1] Pico de Orizaba, also known as Citlaltepetl, is one of the seven most prominent peaks in the world, where prominent is related with the dominance of the mountain over the region[2] (Press & Siever 1982). The Parque National Pico de Orizaba has an area of 192 km^2 enclosing the two volcanic peaks, separated by only 7 km from top to top, and their wide bases. Tliltepetl is an inactive volcanic cone formed 460,000 years ago, much earlier than Citlaltepetl whose present crater was created just 4100

[1] Instituto Nacional de Estadística, Geografía e Informática (INEGI) official figure.
[2] Topographic prominence is defined as the elevation difference between the peak summit and the lowest contour level that encircles that summit but does not encircle any higher summit.

⋆ E-mail: bec@inaoep.mx

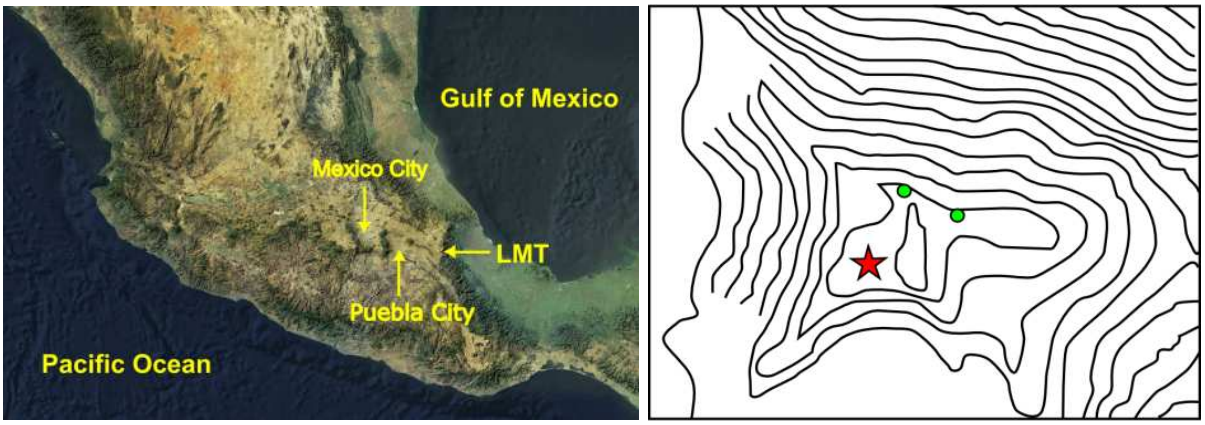

Figure 1. Left: map of Mexico indicating the location of Sierra Negra site [from Conabio site: www.conabio.gob.mx]. Right: site zoom [from INEGI site: www.inegi.org.mx]. The star on the left low corner is the LMT, the open circles show the positions of the meteorological stations. The distance between the stations is 110 m. See the electronic edition of MNRAS for a color version of this figure.

years ago and has a record of activity within the last 450 years, including the flow of 0.1 km^3 of lava in 1566 and a last eruptive event in 1846 (Höskuldsson & Robin 1993; Rossotti 2005). These two peaks are located at the edge of the Mexican plateau which drops at the East to reach the Gulf of Mexico at about 100 km distance, as shown on the left side of Fig. 1. The weather of the site is influenced by the dry weather of the high altitude central Mexican plateau and humid conditions coming from the Gulf of Mexico (Erasmus & Van Staden 2002).

In February 1997 Sierra Negra was selected as the site of the LMT, a 50 m antenna for astronomical observations in the 0.8 - 3 millimeter range. The top of Sierra Negra, defined now by the position of the telescope, on the right side of Fig. 1, has Universal Transverse Mercator (UTM) and geographical coordinates $\{x_{utm} = 677450, y_{utm} = 2100092\}$ and $\{97^\circ\,18'\,51.7''$ longitude West, $18^\circ\,59'\,08.4''$ latitude North$\}$ respectively. The development of the LMT site led to the installation of further scientific facilities benefiting from its strategic location and basic infrastructure like the 5 m radio telescope RT5, a solar neutron telescope and cosmic ray detectors, among others. In July 2007 the base of Sierra Negra, about 500 m below the summit, was chosen as the site of the High Altitude Water Čerenkov (HAWC) observatory, a $\sim 20000\,m^2$ water Čerenkov observatory for mapping and surveying the high energy γ-ray sky. HAWC will be complemented by two atmospheric air Čerenkov telescopes, the OMEGA (Observatorio MExicano de GAmmas) formerly part of the HEGRA array (Konopelko et al. 1999).

The seeing of Sierra Negra was monitored between 2000 and 2003 to quantify the potential of the site for optical astronomy. The site has a median seeing of 0.7", consistent with of a prime astronomical site (Carrasco et al. 2003). The wind velocity at 200 mbar has been analyzed using the NOAA NCEP/NCAR reanalysis database showing that Sierra Negra is comparable to the best observatory sites as Mauna Kea in terms of applying adaptive optics techniques such as slow wavefront corrugation correction (Carrasco et al. 2005), based on the premise that global circulation of atmospheric winds at high altitude can be used as a criterion to establish the suitability of a site for the development of adaptive optics technique as the wind velocity at 200 mbar is strongly correlated to the average wavefront velocity allowing to compute the coherence time τ_o (Sarazin & Tokovinin 2002).

Table 1. Positions of the weather stations relative to the LMT; x increases to the East and y to the North.

	Relative location		
Instrument	x(m)	y(m)	z(m)
LMT	0	0	0
Davis	139	65	–15
Texas	40	105	0

Different scientific facilities seek particular conditions and their dependence on meteorological conditions vary. Among the Sierra Negra facilities we can note:

- the Large Millimeter Telescope requires minimum atmospheric opacity in the millimeter range, which translates in a reduced water vapour column density. According to design specifications, LMT operation at 1 mm require wind velocities below 9 m s^{-1} and the antenna is able to survive winds up to 250 km/h (69.4 m s^{-1}).
- the RT5 5 m radio telescope will operate at 43 and 115 GHz for observations of the Sun. Nighttime work will focus on interstellar masers and monitoring of mm-wave bright active galactic nuclei. RT5 requires absence of clouds in the line of sight.
- optical and atmospheric Čerenkov telescopes require clear nights and relatively low humidity (below 80%) during nighttime.
- water Čerenkov observatories like HAWC seek high altitude environments which allow for a deep penetration of atmospheric particle cascades. They are basically immune to weather, although freezing conditions and large daily temperature cycles are concerns. The same applies to small cosmic ray detectors installed at Sierra Negra summit.

3 INSTRUMENTATION AND LOCATION

The weather data presented here were acquired with three instruments:

(i) **a Davis meteorological station**, hereafter named "Davis", located on a 5 m tower about (139, 65) metres (E,N) from the LMT position. Most of the data shown in this paper comes from this station. It has been operational since October 2000 up to now, and is installed at the base of the former seeing monitor. The station tower is at the edge of a sharp slope facing North East just above the HAWC site -that is approximately 430m E, 1010m N and 500m below the summit. The Davis station consists of temperature and humidity sensors enclosed on a radiation shield, a barometre, an anenometer, a control console and a data logger:

- the temperature sensor is a platinum wire thermistor with a resolution of 0.1°C and a nominal accuracy of ±0.5°C.
- the relative humidity (RH) sensor is a film capacitor element providing a resolution of 1% with an accuracy of ±3% for RH between 0 and 90% and ±4% above 90%.
- the barometre has a resolution of 0.1 mbar and an accuracy of ±0.4 mbar in the measurement of atmospheric pressure.
- the wind monitor consists of a three cup anemometre providing a resolution of 0.4 m s^{-1} and accuracy better than 0.9 m s^{-1} for a wind speed interval between 0.9 and 78 m s^{-1}. [3]

(ii) **a backup Davis station**, hereafter named "Backup", of same model and characteristics as the main Davis station, was temporarily installed at the same position and operated from April 2002 until November 2003, when it ceased functioning.

(iii) **a Texas Electronics weather station**, hereafter named "Texas", consists of:

- a temperature sensor, of model TT-101QR, made of a linear thermistor resistor of 0.1°C resolution and 0.5°C accuracy [4] in the range −34°C to 43°C;
- a humidity sensor consisting of a thin film capacitor with a resolution of 1% and an accuracy of ±3%.
- a radiation sensor made of a solar panel inside a glass dome to obtain maximum cosine response to the Sun's radiation. The nominal range is up to 1400 W/m^2 with a resolution of 1 W/m^2 and 5% accuracy.
- a wind monitor consisting of three anemometre cups providing a resolution of 0.2 m s^{-1} and an accuracy better than 0.5 m s^{-1}.

The Texas weather station has also a barometre, but the readings of atmospheric pressure were found to be spurious.

The Texas station was installed at about (40, 105) metres (E,N) from the LMT and 110 metres apart from the Davis station and 15 m higher than the Davis. Taking the LMT as the reference point the coordinates of both stations are shown in table 1. The relative locations of the LMT and the weather stations are shown in Fig. 1

[3] Specified by the manufacturer in English units: wind speed resolution of 1 mile/hr and nominal accuracy better than 2 mile/hr for an interval between 2 and 175 mile/hr

[4] Specified in English units: the T accuracy is 1°F

4 DATA COVERAGE

The data presented here consist of temperature, atmospheric pressure, relative humidity, wind velocities and radiation records acquired with the Davis and Texas stations using sampling times ranging between 0.5 and 30 minutes. The majority of the data were taken with 1 or 5 minutes sampling. Data on wind direction and dew points were also acquired and will be presented elsewhere, in specific studies of the wind characteristics and atmospheric water vapor content of the site.

Table 2 summarises the temporal coverage of the data, expressed in percentage. The data from the Davis station span from October 30, 2000 to February 18, 2008, with a 70% effective coverage of the 7.3 year sample: data exists for 1986 out of 2668 days. The complete sample contains 2693146 minutes; coverage for day and night are almost equal 1120921 compared to 1122161 minutes. Coverage was ∼ 80% between 2002 and 2006, declining to 36% in 2007. The comparison between the general and the wind data shows that bad weather affects our anenometer less than 5% of the time; in fact our logfile indicates that most of our data losses are not due to bad weather but to logistics.

The Texas station started operation a year and a half later and has a comparable coverage, as shown in Table 3, with a 58% effective coverage corresponding to 1844977 minutes. The data have 3-month gaps in early 2002 and mid-2003. In total we have data for 1584 days out of the 2163 in the period between April 12, 2002 and March 13, 2008. The data of the Texas station have even coverage for day and night: 774698 and 763496 minutes, but are biased towards the dry period. In Table 4 we present the temporal coverage of radiation as it is higher than for the other parameters, in particular for 2004 the coverage is almost twice. The complete solar radiation sample contains 990770 minutes from which 526792 minutes are for the dry season and 463978 for the wet season.

From tables 5 and 6, it is clear that the coverage per hour is fairly homogeneous, varying at most from 56% to 59% for the Texas station, while the coverage per month is more variable, specially for the Texas. The coverage per hour for solar radiation, is shown in table 7. For the early (∼6h) and late afternoon (∼18h) hours the coverage is low mostly due to the variation of the length of the day, for the other hours the maximum difference is 4%.

5 CROSS CALIBRATION

To cross calibrate the two data sets considering the measurement accuracies we compute the best linear regression between the two data sets by minimizing χ^2. The goodness of the fit is given by the correlation coefficient r between the best fit and the data points.

The plots with all the data points and the best fit have more than 10^5 points for each parameter (>2MB). To display them can be misleading because they tend to look as scatter plots. They would suggest that the fitting errors are

Table 2. Data coverage of Davis weather station in percentage.

Month	2000	2001	2002	2003	2004	2005	2006	2007	2008	All
January		65	87	95	65	99	95	77	99	85
February		69	92	99	68	92	77	19	60	76
March		0	99	86	57	70	79	0		56
April		0	85	91	96	87	93	0		64
May		63	99	74	89	78	79	0		69
June		56	94	99	83	88	78	0		71
July		37	97	92	85	77	56	67		73
August		94	98	89	86	73	25	79		78
September		91	93	55	76	98	38	94		78
October	3	97	46	90	90	89	76	24		73
November	14	75	44	81	77	60	60	0		51
December	37	82	78	66	48	36	90	63		63
Year total	27	61	84	85	77	79	70	35	98	70
Dry	26	48	81	86	68	74	82	27	98	66
Wet	54	73	88	83	85	84	59	44		73

Table 3. Data coverage of relative humidity from the Texas weather station in percentage.

Month	2002	2003	2004	2005	2006	2007	2008	All
January		88	89	0	82	64	27	58
February		93	88	0	83	80	91	73
March		100	75	68	93	87	41	77
April	48	84	0	61	95	69		59
May	77	0	40	38	78	10		40
June	88	0	0	84	71	23		44
July	97	0	0	100	100	8		50
August	77	61	0	89	42	0		45
September	85	51	0	99	100	41		63
October	99	73	0	100	85	12		61
November	94	64	0	87	59	68		62
December	98	69	0	74	80	56		63
Year total	85	57	24	67	81	43	52	58
Dry	80	83	42	49	82	71	52	65
Wet	87	31	6	85	79	15	0	51

Table 4. Solar radiation data coverage from the Texas weather station in percentage.

Month	2002	2003	2004	2005	2006	2007	2008	All
January		87	52	60	81	64	28	62
February		93	87	69	83	80	91	84
March		99	57	98	93	88	40	79
April	17	83	8	61	93	72		56
May	39	0	25	37	82	10		32
June	87	0	0	84	71	46		48
July	73	0	29	99	99	8		51
August	77	26	99	88	43	32		61
September	84	51	50	99	99	59		74
October	99	74	44	99	85	11		69
November	93	64	45	86	66	69		71
December	97	68	46	74	81	56		70
Year	73	52	44	80	81	48	52	62
Dry	68	83	49	75	83	72	52	70
Wet	76	24	41	84	80	27	0	55

Table 5. Hourly data coverage of Davis weather station.

	Jan	Feb	Mar	Apr	May	Jun	Jul	Aug	Sep	Oct	Nov	Dec	Per Hour
0h	85	76	55	65	69	72	74	78	78	73	52	62	70
1h	84	77	55	64	69	72	75	78	77	73	52	62	70
2h	85	77	56	64	69	72	74	78	77	73	52	62	70
3h	85	77	55	64	69	73	74	78	78	73	52	62	70
4h	84	76	55	63	69	73	74	78	78	73	52	62	70
5h	85	77	56	63	70	73	74	78	78	73	51	62	70
6h	85	77	56	64	70	72	74	78	78	73	51	62	70
7h	85	77	56	64	70	72	74	78	78	74	52	63	70
8h	85	77	57	64	69	72	73	79	78	74	52	63	70
9h	85	75	56	63	69	71	73	78	78	72	51	63	69
10h	86	75	56	64	68	70	72	77	78	72	51	63	69
11h	86	76	57	65	69	71	73	77	78	72	51	63	70
12h	86	76	56	64	69	71	72	77	77	72	52	63	69
13h	86	76	56	65	68	70	72	77	76	72	52	63	69
14h	86	75	56	64	68	70	72	77	77	73	52	62	69
15h	87	74	56	65	68	70	72	77	77	73	52	62	69
16h	87	74	56	66	69	70	72	78	77	72	51	63	70
17h	86	76	56	66	69	70	72	78	77	73	52	63	70
18h	86	76	56	66	69	70	72	77	77	72	51	62	70
19h	86	75	56	65	69	70	72	78	78	73	51	62	70
20h	85	76	56	65	69	69	71	77	77	72	51	62	69
21h	85	75	56	65	68	70	72	76	78	72	50	63	69
22h	85	75	55	64	69	70	72	78	77	72	51	63	69
23h	85	75	55	65	68	71	73	78	78	71	52	63	69
Per Month	85	76	56	64	69	71	73	78	78	73	51	63	**70**

Table 6. Hourly data coverage of humidity from the Texas weather station.

	Jan	Feb	Mar	Apr	May	Jun	Jul	Aug	Sep	Oct	Nov	Dec	Per Hour
0h	59	67	77	56	40	44	51	45	63	61	60	63	58
1h	59	67	77	56	39	42	51	45	63	60	60	62	57
2h	59	67	77	56	39	42	51	45	63	60	60	62	57
3h	58	67	77	56	39	42	51	44	63	59	60	62	57
4h	58	67	77	56	39	42	51	44	63	59	60	62	57
5h	57	67	77	56	39	42	50	43	63	59	60	62	56
6h	57	67	77	55	39	42	49	42	62	59	59	62	56
7h	56	67	77	56	40	43	49	43	62	59	59	62	56
8h	57	67	77	60	41	43	49	45	62	59	61	62	57
9h	57	67	78	61	42	43	49	45	63	59	62	62	57
10h	57	67	78	61	41	44	50	45	63	59	62	62	58
11h	57	67	77	61	41	44	51	44	62	60	63	62	58
12h	58	68	77	61	40	44	51	45	62	62	64	62	58
13h	59	69	76	62	41	44	51	46	63	64	65	63	59
14h	59	70	77	62	42	45	51	46	63	64	64	64	59
15h	60	70	77	62	42	46	51	45	63	64	64	64	59
16h	60	69	78	63	42	46	51	45	62	64	65	64	59
17h	60	69	78	63	42	46	51	45	62	65	65	65	59
18h	60	68	78	63	42	46	51	46	63	64	65	65	59
19h	60	68	77	63	41	46	51	46	63	64	64	64	59
20h	60	68	77	63	40	46	51	46	62	64	64	63	59
21h	60	69	77	60	40	46	51	45	62	63	63	63	59
22h	60	69	77	59	39	46	51	45	62	63	61	63	58
23h	60	68	77	58	39	46	51	45	62	62	61	63	58
Per Month	58	68	77	59	40	44	50	45	63	61	62	63	**58**

Table 7. Hourly data coverage of radiation from the Texas weather station.

	Jan	Feb	Mar	Apr	May	Jun	Jul	Aug	Sep	Oct	Nov	Dec	Per Hour
6h	0	2	29	48	30	45	43	36	37	24	12	0	25
7h	51	80	88	63	31	46	50	59	74	66	67	66	61
8h	60	83	88	64	32	46	50	61	74	66	68	70	63
9h	61	82	88	64	33	46	51	61	75	66	69	70	64
10h	61	82	88	64	32	47	51	61	75	66	70	70	64
11h	61	83	87	64	32	48	52	60	74	67	70	70	64
12h	62	84	87	65	32	48	52	61	73	70	71	70	64
13h	62	85	87	65	32	48	52	63	73	72	72	70	65
14h	63	86	87	65	33	49	52	63	74	72	72	72	65
15h	63	86	87	66	33	50	52	62	74	71	72	72	66
16h	64	86	88	66	33	50	52	63	73	72	73	72	66
17h	64	86	88	66	33	50	52	63	74	72	67	64	65
18h	7	28	41	39	26	49	52	59	45	12	0	0	29
Per Month	62	84	87	64	32	48	51	61	74	69	71	70	**64**

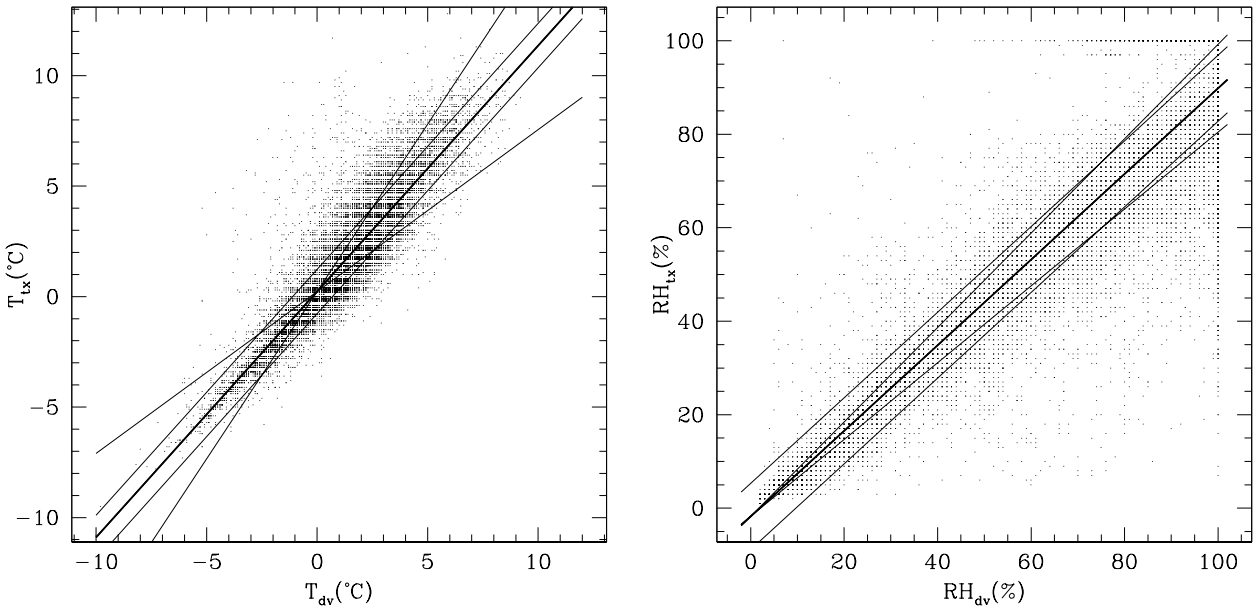

Figure 2. Fits between the Davis and the Texas stations for temperature (right) and RH (left). The fit with the best slope and zero point is indicated with a bold line. The fits adding $\pm 1\sigma$ error to each fitting parameter are also shown: the two parallel fits to the best one correspond to 1σ and -1σ in the ordinate; the other two fits correspond to 1σ and -1σ error in the slope.

underestimated as it is impossible to distinguish if in a given position there is one or 10^3 points. We decided to present plots with 1/10 of the data points randomly chosen as in this case the points tend to be located where the density of data is larger and, on the other hand, the files are handled.

For a given plot, the equality between the Davis and Texas data corresponds to a straight line at 45°, not shown. We present the best fit and zero point (bold line) and the fits obtained adding the 1σ error to each parameter.

We report the fits -and the statistics- with two decimal digits as the determination of a statistical value can be made with higher accuracy than the nominal resolution of the instrument for data with high signal to noise ratio (S/N). In our analysis the high S/N is due to a very large data set.

Subscripts $_{dv}$ and $_{tx}$ stand for the Davis and Texas stations, respectively, for any of the compared parameters: temperature T in $^\circ C$, relative humidity RH in per cent, and wind speed w in m s^{-1}.

5.1 Temperature

We compared temperature data from both stations registered with same times, allowing for up to a one minute difference between clocks. The 233985 registers common to the Davis and Texas station are in fair agreement, with a correlation of 0.90 for the linear fit,

$$T_{tx} = (1.11 \pm 0.4)\, T_{dv} + (0.23 \pm 1.0)^\circ\mathrm{C}, \qquad (1)$$

the rms scatter around the fit is 1.23°C, which is 1.7σ, where σ=0.7 is the combined error accuracy of both stations. The data points with the best fit and the fits obtained adding $\pm 1\sigma$ are shown on the left side of Fig. 2.

Table 8. Linear fits, RH(Texas) = slope * RH(Davis) + intercept, to common data on relative humidity.

Sample	slope	intercept % ±7.07	rms %	correl	N_{points}
2002	0.97 ± 0.10	−1.00	11.5	0.94	72025
2003	0.94 ± 0.10	−2.22	9.0	0.96	52103
2004	0.90 ± 0.10	−1.90	9.2	0.96	12705
2005	0.88 ± 0.08	−4.27	11.2	0.88	33024
2006	0.89 ± 0.09	−4.63	9.1	0.96	36622
2007	0.82 ± 0.01	−0.82	11.8	0.93	3284
2008	0.89 ± 0.09	−5.78	8.9	0.94	2354
All	0.92 ± 0.09	−1.77	11.2	0.94	212117

Relation (1) leads to a larger range of temperatures for the Texas station than for the Davis one and differences ~ 1°C for *extreme* temperature, $|T| \gtrsim 10$°C. Additionally, the comparison between the Davis station and the Backup station gives a fit with a slope of 1.03, intercept of 0.03 and r =0.99. We consider the temperature data from different stations to be consistent with each other.

5.2 Relative humidity

Even though both stations have similar humidity sensors, we found significant systematic differences in simultaneous measurements. Some of these might be attributed to local differences in humidity, due to fog moving accross the site, as the stations are located 130 m apart. The common data are well correlated ($r = 0.94$) with a linear fit marginally consistent with a one to one relation,

$$\mathrm{RH}_{tx} = (0.92 \pm 0.09)\,\mathrm{RH}_{dv} - (1.8 \pm 7.1)\%. \qquad (2)$$

The values from the Davis station tend to be 10% higher than those from the Texas. The comparison between the Backup and Davis stations gives a similar fit, of slope 0.91, with a correlation equal to 0.99, being more consistent with the data from the Texas weather station. The data points with the best fit (bold line) and the fits obtained adding $\pm 1\sigma$ are shown in Fig. 2, on the right hand side.

Of further significance is the variation of this fit with time, shown in Table 8. The fits for 2002 and 2003 are compatible with equal measurements from both stations, $\mathrm{RH}_{tx} = \mathrm{RH}_{dv}$, while those onwards from 2005 become deviant. The measurements of the stations were similar at earlier times and diverged with time. The slope drifted from 0.97 ± 0.10 in 2002 to 0.82 ± 0.10 in 2007, resulting in larger humidity measurements for the Davis station, by about 10%. In fact, the Davis weather station data show such a trend. The best fit of the yearly median RH_{dv} *vs.* year shows a 4% increase per year with a correlation coefficient of 0.91. However, the Texas station does not show this trend as the best fit of the yearly median RH_{tx} *vs.* year shows a slope of −2.1% per year and a correlation coefficient of −0.25.

To complement the relative humidity analysis we used the RH monthly mean data at 600 mb provided by the National Center for Environmental Prediction/National Center for Atmospheric Research (NCEP/NCAR) Reanalysis project. The NCEP data, included in Fig. 4 in dotted lines, follow the same trend as those measured in situ, but with lower values by up to 40%. The offset can be explained by the fact that some variables as RH are partially defined by observations but also are strongly influenced by the local topography and the characteristics of the NCEP analysis model, as pointed out by Kalnay et al. (1996). Even with an offset these data can be used to look for a tendency. In the case of annual trend, the NCEP reanalysis data does point to an increase of RH of 0.9% per year with a correlation coefficient of 0.7. The data actually shows a 1% per year decrease in RH from 2001 (39%) to 2004 (36%) followed by increased mean values of 42% between 2005 and 2007. This increase is not comparable to the Davis one. We conclude that the RH sensor of the Davis station drifted with time proving higher values than the real ones.

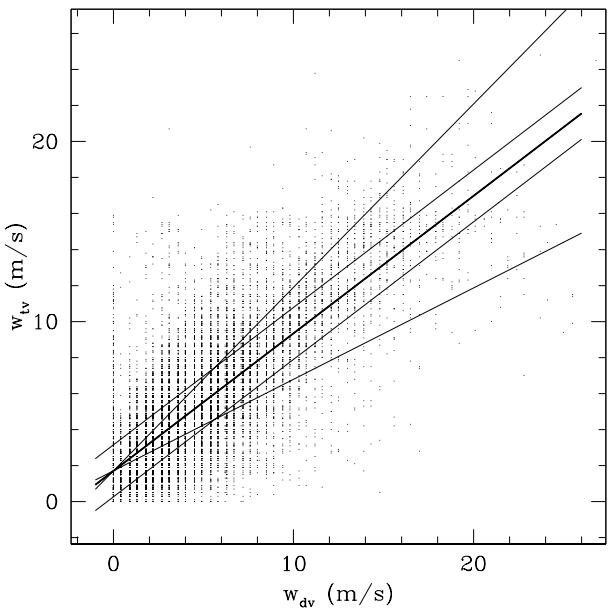

Figure 3. Wind speed: fit with a best slope and zero point is indicated as a bold line. The fits adding $\pm 1\sigma$ error to each fitting parameter are also shown: the two parallel fits to the best one correspond to 1σ and -1σ in the ordinate; the other two fits correspond to 1σ and -1σ error in the slope.

5.3 Wind velocity

Simultaneous wind measurements from both stations follow the best fit,

$$w_{tx} = (0.76 \pm 0.26)\, w_{dv} + (1.7 \pm 1.4)\mathrm{m\ s^{-1}}, \qquad (3)$$

with a correlation coefficient of 0.75. The simultaneous outputs from the anemometres are less correlated than the temperature and humidity data. The Davis weather station tends to give lower values. The fit marginally excludes $w_{tx} = w_{dv}$ in the parameter 1σ error contour. The rms deviation of the fit is 2.29 m s^{-1}, more than twice the combined measurement error of 1.02 m s^{-1}. The data points with the best fit and the fits obtained adding $\pm 1\sigma$ are shown in Fig. 3.

The median velocities of both stations are below the LMT operation threshold of 9 $m\ s^{-1}$. Furthermore, look-

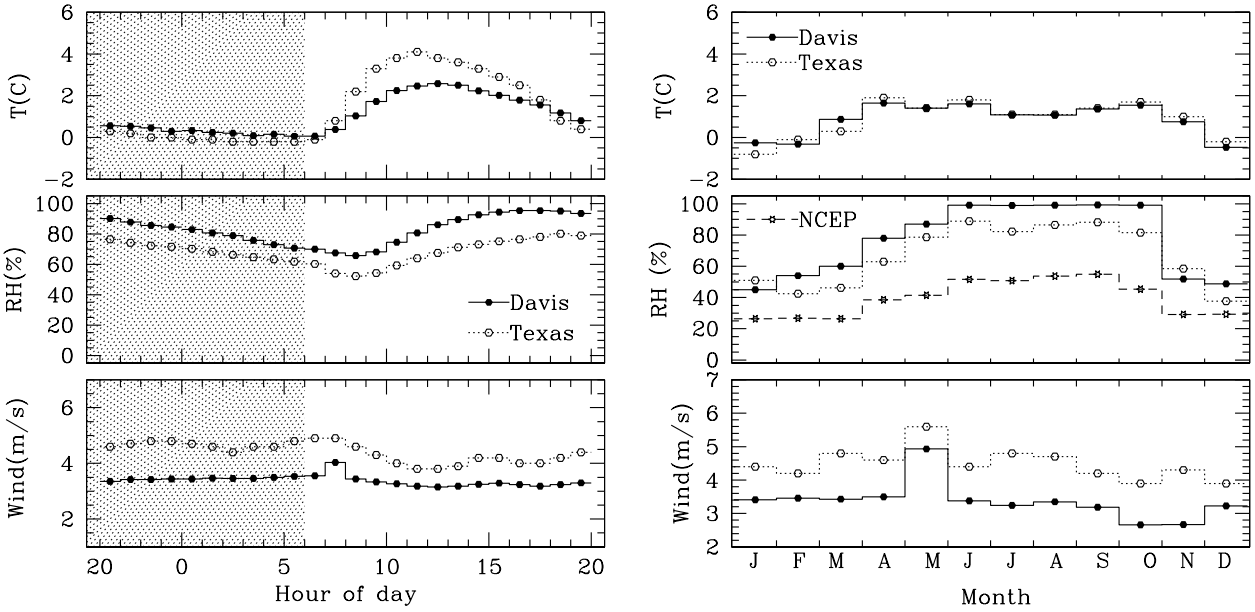

Figure 4. Comparison between data from the Davis and Texas weather stations. Left: median values per time of day. Solid lines and filled circles represent the Davis stations; open circles and dotted line Texas. Here, the RH very low values measured during the dry season, are blended with the high values during the wet season. Right: the same for monthly values, in the RH plot the curve with stars corresponds to the NCEP Reanalysis model for a 600 mbar pressure level.

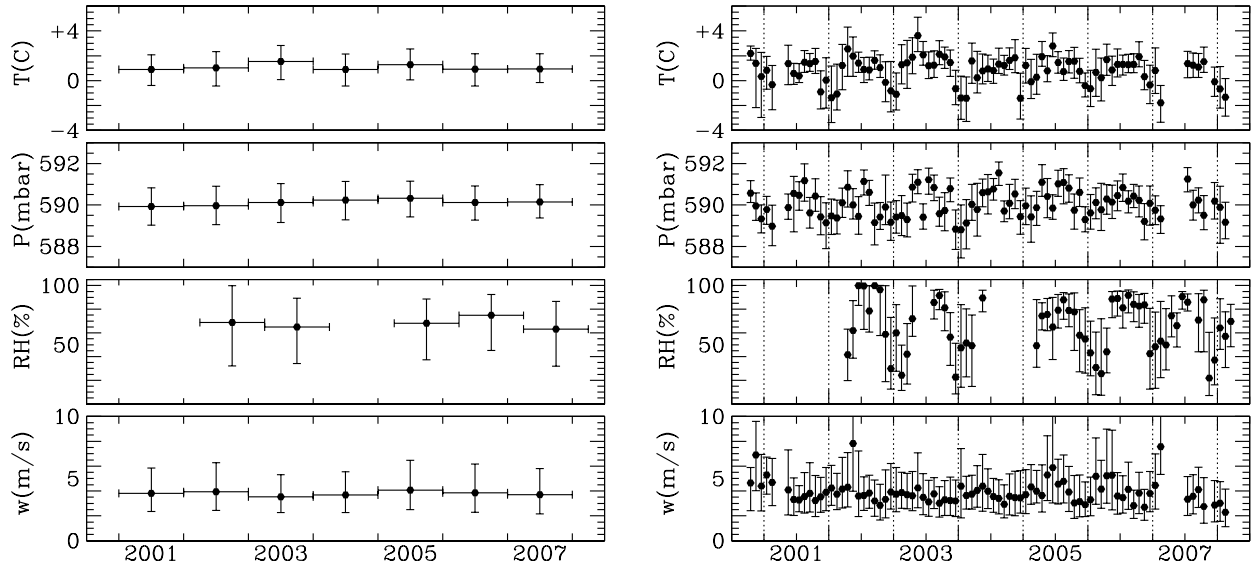

Figure 5. Statistics for all the data, points are medians with bars going from the first to the third quartile. Left: yearly statistics. Right: monthly statistics. The stability of the parameters is appreciated in the annual median values. However more information is extracted from the monthly statistics, in particular in the case of RH that is very low during the dry seasons months as we discussed in detail in the RH section.

ing at the distributions we note that the percentage of wind speeds below the LMT operation threshold are very similar for both stations. We compared the best fit with the fit $w_{tx} = w_{dv}$ and we found that the zero point in the best fit cancels the effect of the different slope giving the same statistical behaviour of both data, although not necessarily simultaneous values. The fact that the statistical behaviour of the two data sets is similar supports the premise that there can be genuine differences in wind speeds due to the topography of the mountain top.

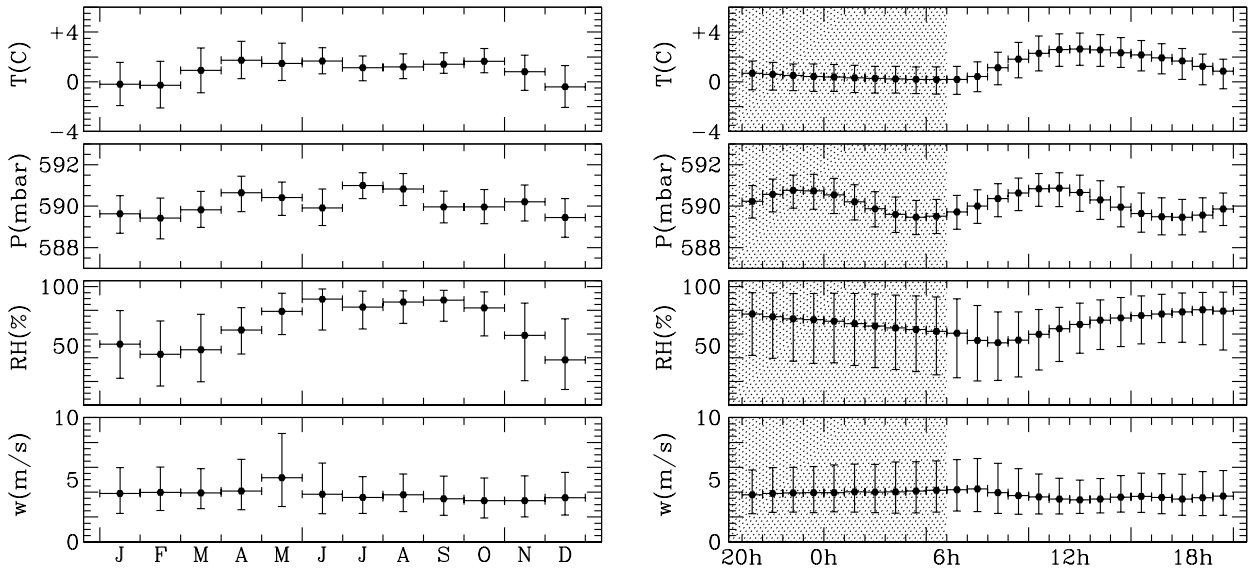

Figure 6. Left: monthly statistic. Each point corresponds to the monthly median for all the years with the bars going from the first to the third quartile. RH is the parameter that shows the strongest seasonal dependence. Right: hourly statistics of all data. The points are the median values and the bars go from the first to the third quartile. The daily cycle is recognizable for all the parameter but in the case of RH the very low values measured during the dry season, are blended with the high values during the wet season.

6 DATA ANALYSIS AND RESULTS

Median and quartile values were computed for the different parameters and datasets. The data points were weighted by sampling time. A time interval larger than 16 minutes without data is considered a gap. We did not compensate for gaps in the data.

The samples were divided in different subsamples for their study, defined as follows: *daytime* is the 10 hr interval between 8:00am and 5:59pm; *nighttime* ranges from 8:00pm to 5:59am. These two definitions avoid the transition times of sunrise and sunset to analyse the weather under stable conditions. The *dry season* is the 181 day period from November 1st to April 30; the *wet season* goes from May 1st to October 31st, covering 184 days. The time span period of the Davis data comprises 1378 dry season days (978 with data) and 1290 wet season days (1008 with data); the time span period of the Texas data comprises 1059 dry season days (889 with data) and 1104 wet season days (695 with data).

6.1 Parameter statistics - seasonal and diurnal

The data statistics of the meteorological parameters, except solar radiation, are summarised in table 9, for the entire samples and for the day/night, dry/wet season subsamples. The columns indicate from left to right, coverage percentage, minimum, first, second, third quartile values (q_1, q_2, q_3) and maximum. Temperature, atmospheric pressure and wind speed statistics are from the Davis data, while statistics for relative humidity statistics were computed for the Texas weather station. The "all", "day" and "night" statistics were estimated compensating for the uneven seasonal coverage of the Texas data, using 695 days out of the 889 days dry season

Table 9. Weather data statistics. Temperature, pressure and wind speed are from the Davis station while relative humidity is from the Texas weather station, as explained in the text. Quartiles are estimated with an accuracy of $\Delta x/100$, where Δx is the sampling of the parameter under consideration.

	cov(%)	min	q_1	median	q_3	max
Temperature (°C)						
All	71	–10.6	–0.30	1.07	2.32	11.8
Dry	71	–10.6	–1.42	0.34	2.10	9.9
Wet	72	–4.8	0.38	1.39	2.48	11.8
Day	71	–10.4	0.73	2.12	3.36	11.8
Night	71	–10.2	–0.82	0.35	1.37	6.7
Atmospheric pressure (mbar)						
All	71	580.2	589.19	590.11	590.99	594.7
Dry	71	581.6	588.85	589.82	590.74	594.3
Wet	72	580.2	589.51	590.39	591.19	594.7
Day	71	580.8	589.26	590.22	591.14	594.7
Night	71	580.2	589.22	590.13	591.00	594.7
Relative humidity (%)						
All	58	1	36.73	68.87	92.59	100
Dry	65	1	20.82	50.92	78.52	100
Wet	51	2	64.86	84.92	96.18	100
Day	58	1	40.70	68.19	88.73	100
Night	58	1	33.18	69.35	93.96	100
Wind speed (m s^{-1})						
All	69	0	2.31	3.77	5.88	36.2
Dry	68	0	2.36	3.80	5.91	36.2
Wet	70	0	2.27	3.74	5.85	35.8
Day	69	0	2.28	3.57	5.45	35.8
Night	68	0	2.36	3.98	6.18	35.8

data. For solar radiation, the subdivision "day" and "night" become meaningless. The results of the analysis of solar radiation data, including the influence of daytime cloud cover, are described in subsection §7.

Table 10 displays the annual statistics of each parameter, considering also the dry and wet seasons. In Fig. 5 we plot the median values of the measured parameters per year and per month, with bars going from the first to the third quartile. Fig. 6 shows the statistics of the data folded per month and per hour of day, in order to show the seasonal and daily modulations.

6.2 Temperature

According to the Davis weather station, the median temperature for the site is 1.07°C, with quartile values of −0.30°C and 2.32°C. The extreme temperatures recorded by the Davis station on site are relatively mild: the minimum temperature in the data is −10.6°C while the maximum 11.8°C. The Texas station registered the same median temperature, but with somewhat larger variations and more marked extremes: −13.3°C and 14.4°C. As it would be expected that both stations register the same extreme temperature, it is required to perform some experiments to determine if these differences are real or are due to the distinct temperature sensors sensitivity to extreme conditions. We plan to carry out such experiments. In any case the temperatures at the site do not show large variations.

The daily cycle, quantified as the difference between the night and day medians, is 1.77°C, going from 0.26°C to 2.03°C respectively. A similar value is obtained for seasonal variations: the median and third quartile (q_3) values for dry/wet differ by only 1.76°C and 1.09°C respectively. The lowest quartile does show a larger -but still mild- difference, close to 2°C. In Fig. 6 the amplitude of the curve between the lowest median, -0.22°C at 5am, and the highest median, 4.15°C at 11pm, is 4.37°C. The coldest month is December, with a median of −0.59°C, 2.5°C below the warmest month, June, with a median of 1.91°C.

Temperature distributions are shown in the cumulative histograms on the left panel of Fig. 7. The distributions for nighttime, daytime, dry and wet seasons are shown as indicated. The temperature differences due to the diurnal cycle are larger for values above the median while the seasonal temperature differences are larger for values below the median. The right hand side panel of the same figure shows in a grey scale diagram the medians per hour and month. Temperatures are at their lowest during the nights of the dry months, specifically between December and February, and highest around or just after noon between April and June. Note that the period between July and September is not warmer than April and May, due to the effect of rain.

If we consider the altitude of the site and the temperature gradient of a standard atmosphere model, $dT/dz = -6.5$°C/km, the corresponding sea-level temperature is $T_0 = 30.9$°C, about 16°C above the standard atmosphere base value. This is clearly an effect due to the low latitude, which results in a warmer temperature at a high altitude site. A final remark is that the site presents a good degree of thermal stability, beneficial for scientific instruments: thermal stability will help the performance of the LMT, designed to actively correct its surface to compensate for gravitational and thermal deformations.

6.3 Atmospheric pressure

The barometre of the Texas weather station did not provide meaningfull data and these had to be discarded. We discuss only the data from the Davis weather station. To verify the calibration of the Davis barometre we performed a comparison with a basic water barometre, for about 3 hours during daytime, obtaining a pressure of 594 mbar, in very good agreement with the Davis barometre reading of 592.4 mbar. Therefore, the Davis weather station gives readings accurate to within 2.4 mbar.

The site presents a low atmospheric pressure which is characteristic of a high altitude site. The median is 590.11 mbar with a daily cycle of 1.45 mbar, as measured by the difference between the median of the 4 am sample (589.36 mbar) and that of the 11am data (590.81 mbar), displayed in Fig. 6. The daily cycle is in fact a double 12 hour cycle, with maxima at 11h and 23h and minima at 5h and 17h. This semidiurnal pressure variation of a few mbar is well known for low latitude zones. It is associated with atmospheric tides excited by heating due to insolation absorption by ozone and water vapor (Lindzen 1979). The yearly cycle is not as well defined, see Fig. 10, with relative minima in February (589.37 mbar), June and December, and maximum value in July (590.87 mbar), for a peak to peak amplitude of 1.5 mbar.

High and low pressure are usually related to good and bad weather, respectively. The largest pressure recorded on site is 597.4 mbar, 3.8 mbar above the median, just before midnight on the 17/8/2001 and again at noon 18/8/2001. The weather was dry as relative humidity values were 18% and 22% respectively with temperatures of 1.4°C and 4.7°C. We note that while the weather is usually poorer in the wet season, these good conditions happened in August, indicating that good observing conditions can happen any time of year; the largest atmospheric pressure during the dry season occurred on 7/3/2004 at 10:35 am, when the weather record indicated a pressure of 594.3 mbar, temperature of 5.9°C and a relative humidity of just 12%.

The lowest pressure corresponded to what has presumably be the worst weather on site: the relatively close passage of hurricane Dean, on 22/8/2007. At 4:30am when the pressure dropped to 580.2 mbar, practically 10 mbar below the site median, with a temperature of −0.1°C and relative humidity of 92%. The same day registered the lowest daytime pressure, 580.8 mbar, at 10am, when the temperature had *dropped* to −0.3°C. Bad weather occasionally occurs early in the year, like on the 17/1/2004 at 6:20 am when the pressure reached its lowest dry season value, 581.6 mbar, with a temperature of −3.7°C and 85% relative humidity.

As shown in Fig. 8, there is no significative difference between the cumulative distribution of atmospheric pressure values between day and night, presumably because of the actual 12 hour cycle. The seasonal distributions show that pressure tends to be 0.57 mbar lower during the dry season compared to the wet season. The grey scale diagram in Fig. 8 shows that the main seasonal effect on pressure seems to be a shift the daily cycle to later hours in June - July; the

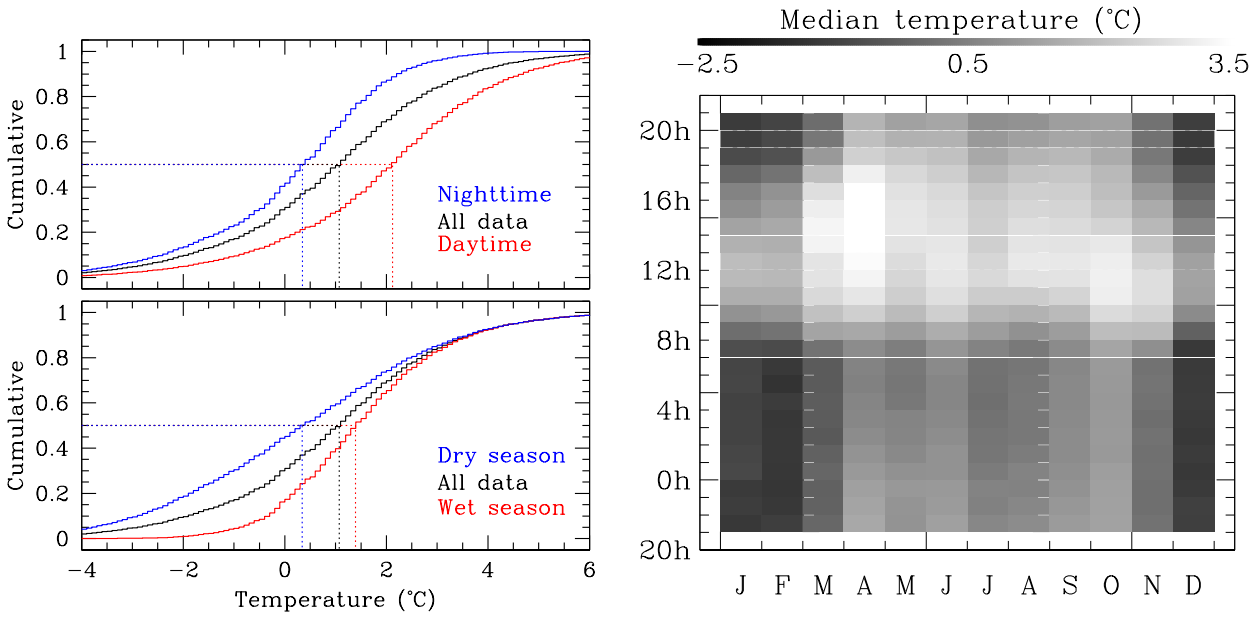

Figure 7. Left: the temperature distribution for the whole data set is shown in black with a median of 1.07°C. The distributions for nighttime, daytime, dry and wet season are shown as indicated. The median values are 0.35°C, 2.12°C, 0.34°C and 1.39°C respectively. Right: a three dimensional representation of the temperature behaviour where the grey scale intensity corresponds to the temperature median for a given month and hour. The annual and daily cycle are apparent in the horizontal and vertical structure of the figures, behaving as expected. See the electronic edition of MNRAS for a color version of this figure.

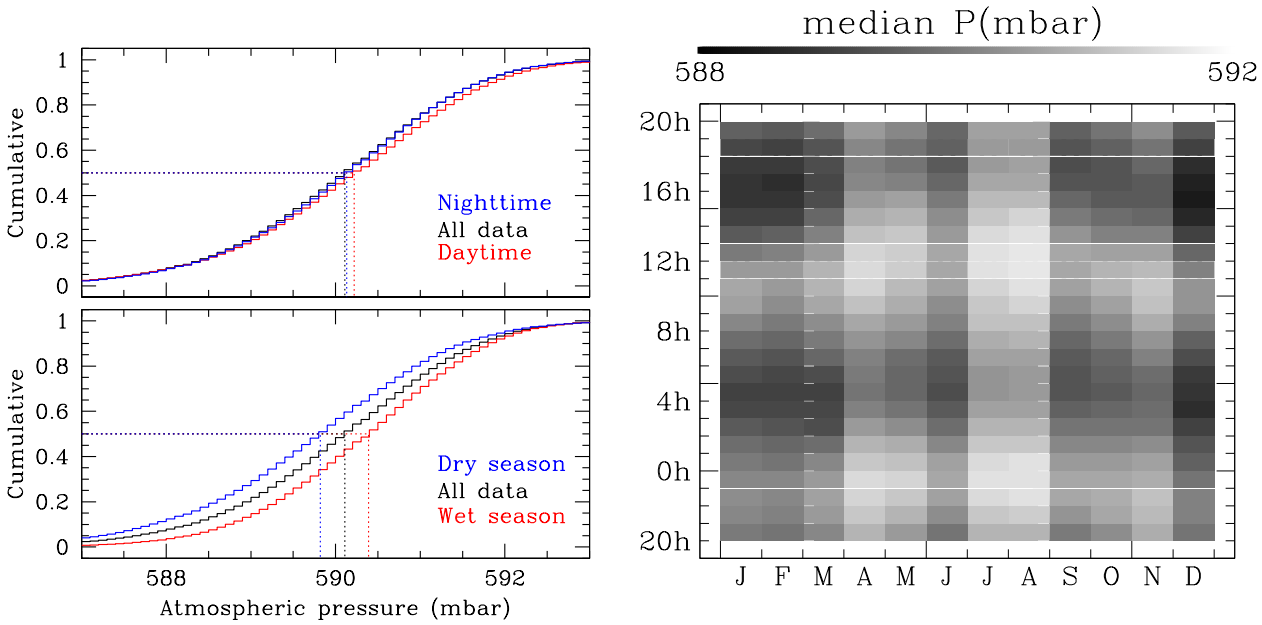

Figure 8. Right: The atmospheric pressure distribution for the whole data set is shown in black with a median of 590.11 mbar. The distributions for nighttime, daytime, dry and wet season are shown as indicated. The median values are: at nighttime 590.13 mbar, at daytime 590.22 mbar, during the dry season 589.82 mbar and during the wet season 590.39 mbar. Left: a three dimensional representation of the atmospheric pressure, the intensity corresponds to the atmospheric pressure median value for a given month and hour. The daily and yearly cycle are clearly recognizable. See the electronic edition of MNRAS for a color version of this figure.

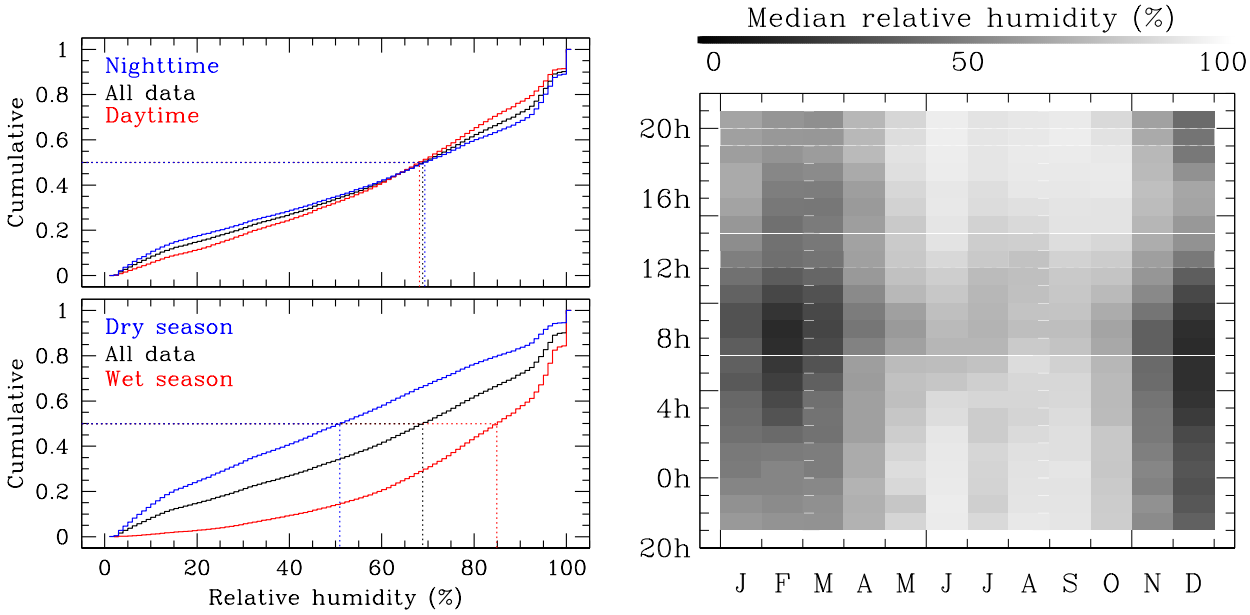

Figure 9. Top left: the relative humidity distribution for the whole data set, for nighttime and for daytime have been included only for completness as the RH is strongly seasonal dependent. Bottom left: distributions for the dry and the wet seasons: the RH median during the dry season is 50.92% while during the wet season is 84.92%. Right: a three dimensional representation of the relative humidity behaviour where the intensity corresponds to the RH median value for a given month and hour. The seasonal differences are clearly appreciated. See the electronic edition of MNRAS for a color version of this figure.

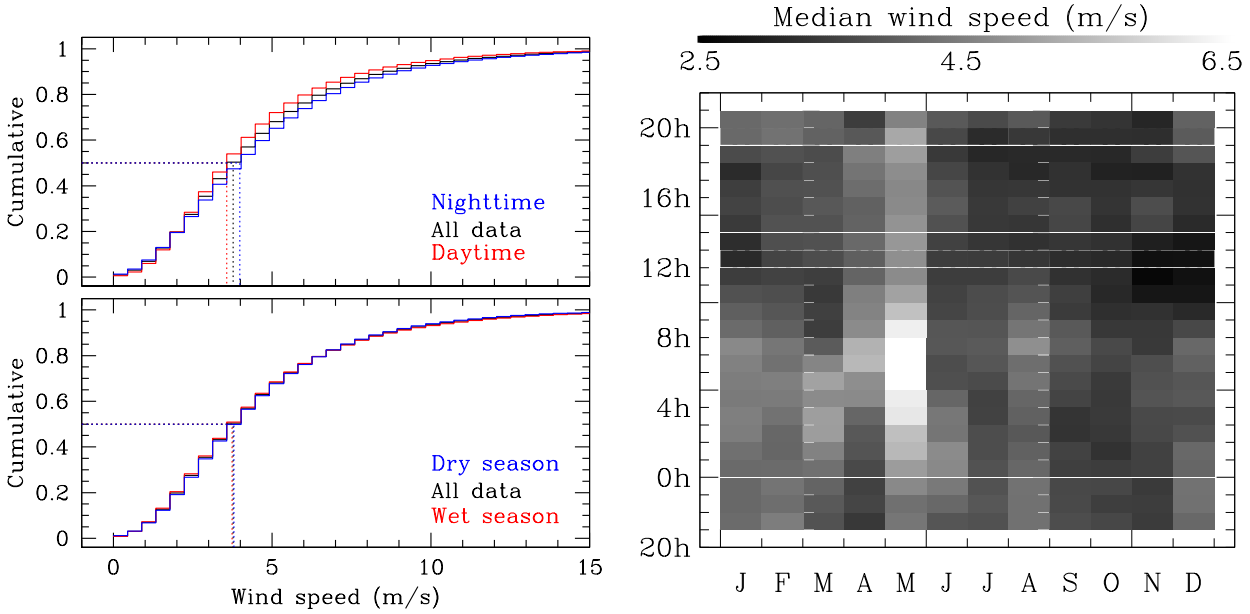

Figure 10. Right: The wind velocity distribution for the whole data set is shown in black with a median of 3.77 m s^{-1}. The distributions for nighttime, daytime dry and wet seasons are shown as indicated. The wind velocity median values are: at nighttime 3.98 m s^{-1}, at daytime 3.57 m s^{-1}, in the dry season 3.80 m s^{-1} and in wet season 3.74 m s^{-1}. Left: a three dimensional representation of the wind speed, the intensity corresponds to the wind velocity median for a given month and hour. The winds are stronger during the nights. See the electronic edition of MNRAS for a color version of this figure.

Table 10. Median values of the meteorological parameters per year and season .

Parameter	2001	2002	2003	2004	2005	2006	2007
Temperature (°C)	0.90	1.02	1.54	0.89	1.28	0.91	0.93
Dry season	−0.10	0.25	0.80	0.10	0.87	0.32	0.08
Wet season	1.25	1.28	1.93	1.18	1.57	1.35	1.25
Pressure (mbar)	589.93	589.97	590.12	590.24	590.32	590.12	590.15
Dry season	589.38	589.81	589.85	589.75	590.12	589.89	589.84
Wet season	590.29	590.11	590.42	590.59	590.47	590.40	590.40
Relative Humidity (%)		68.86	65.06	(74.50)	68.10	74.80	63.13
Dry season		42.01	53.53	(49.21)	49.94	52.69	58.30
Wet season		99.56	86.07	(89.50)	78.95	85.28	81.47
Wind (m s^{-1})	3.81	3.94	3.54	3.68	4.07	3.86	3.71
Dry season	4.28	4.01	3.60	3.78	3.74	3.95	3.81
Wet season	3.49	3.88	3.48	3.60	4.42	3.74	3.66

minima move from 4 am and 4 pm in December/January to 6 am/6 pm in June/July.

The temperature and atmospheric pressure agree with a standard atmosphere model,

$$T(z) = T_0 - \theta z, \quad P(z) = P_0(1 - \theta z/T_0)^{\alpha}, \qquad (4)$$

with the usual temperature gradient of a standard atmosphere, $\theta = -dT/dz = 6.5^{\circ}\mathrm{C\,km^{-1}}$, and the constant $\alpha = \mu m_H g/k\theta \simeq 5.256$, with m_H the atomic mass unit, g the acceleration of gravity, k the Boltzmann constant, $P_0 = 1013.25$ mbar and $\mu = 28.9644$ is the mean atomic mass of air. The data departure from the standard model requires a warmer base temperature, $T_0 = 31^{\circ}\mathrm{C} \simeq 304K$, which results in $T(4.6\ \mathrm{km}) = 1.1^{\circ}\mathrm{C}$ and $P(4.6\ \mathrm{km}) = 588.2$ mbar, close to the measured value. A warm standard atmosphere model appears reasonable for the site although it would be convenient to validate it with measurements of pressure and temperature at different elevations.

6.4 Relative humidity

The median RH is 68.87% with quartile values of 36.76% and 92.59%. The RH values for day and nighttime are 68.19% and 69.35% . When folded by months, the data show a clear seasonal modulation with lower values between November and March, $\lesssim 50\%$ and higher humidity between June and October with a median $\sim 90\%$ as illustrated in Fig. 6. A second clear trend is an increase of the RH at around 8h to reach a maximum at 18h, ∼80 %. Once the Sun sets the RH starts decreasing to reach its minimum value of 49%. Nevertheless, it must be mentioned that for the daily cycle plot the very low RH values measured during the dry season are merged with those obtained during the wet season at the same hour.

The cumulative distributions of RH are shown on the left side of Fig. 9 where the seasonal differences are better appreciated. For the dry season the first, second and third quartile are 20.82% 50.92% and 78.52%. In contrast for the wet season the corresponding values are 64.86%, 84.92% and 96.18%. The right hand side of the same figure shows the median per hour and month in a grey scale. For November, December, January and Februrary, the driest times are from about 8:pm up to noon while for February, March, April and May the RH is lowest from dawn up to midday.

6.5 Wind velocity

Wind velocity is an important factor for the Large Millimeter Telescope, specified to perform at $\lambda \leqslant 1$ mm for wind velocities below 9 m s^{-1}. Both stations give similar percentage of data below the critical value of 9 m s^{-1} (Davis: 91.5%; Texas: 87.7%). The Davis weather station has two wind values in each data record: one ("wind") corresponding to a mean value acquired during the sampling interval ($\geqslant 1$ minute) and a second one ("whigh") corresponding to the maximum value during the same time interval. The median value of whigh is 6.03 m s^{-1} and whigh$\geqslant$ 9 m s^{-1} for 22% of the time.

The wind is fairly constant at the site, with a mild decrease less than 1 m s^{-1} during daytime compared to nighttime. Differences between months are also small, except for a marked increase in wind velocities during the month of May ($\sim$ 1.5 m s^{-1}), noted by both datasets, and a small decrease ($\lesssim$ 0.5 m s^{-1}) of wind velocities in the last months of the year.

The wind distributions are shown in Fig. 10 in black for the whole data set; for nighttime, daytime, dry and wet seasons as marked. In the 3-D plot a seasonal pattern can not be as clearly identified as in the case of other parameters but we can still notice that the wind is slightly higher during the nights and the effect is more pronounced during the winter months. A special mention deserves the strong winds in one year in May as can be seen from Fig. 6. The daily cycle is better appreciated in the right panel of the same figure if we look at the third quartile pattern.

The LMT has two other specified wind limits: operations at any wavelength are to stop if wind velocities reach 25 m s^{-1} and the telescope has to be stowed. In the extreme, the design survival wind speed is 70 m s^{-1} ($\simeq$250 km/h). The two data sets show extremely rare wind velocities above 25 m s^{-1}, with whigh exceeding that value 0.3% of the time. The largest wind speed registered so far corresponded to the storm recorded on the 22$^{\mathrm{nd}}$ of February 2002, with whigh = 42.5 m s^{-1}. More recently the near passage of hurricane Dean in August 2007 gave peak wind speeds of

40.7 m s^{-1}, the highest endured successfully by the Large Millimeter Telescope prior to the installation of its stow pins.

7 SOLAR RADIATION AND INFERRED CLOUD COVERAGE

Solar radiation data was acquired by the Texas weather station between April 25, 2002 and March 13, 2008. The coverage for this time interval was 62% (Table 3), with due consideration of the diurnal cycle. The data are output as time ordered energy fluxes in units of W/m^2. We obtain daily plots of the radiation flux which show the expected Solar cosine modulation. We present here a preliminar analysis regarding a method to retrieve the cloud coverage from the radiation data.

The radiation flux at ground level is modulated by the position of the Sun according to

$$F(t) = F_{\odot} \cos\theta_{\odot}(t)\, \psi(t)\,, \qquad (5)$$

where $F_{\odot}$ is the solar constant, which for working purposes we take as exactly equal to 1367 W/m^2; $\theta_{\odot}$ is the zenith angle of the Sun and $\psi(t)$ is a time dependent factor, nominally below unity, which accounts for the instrumental response, the atmospheric absorption on site and the effects of the cloud coverage on the radiation transfer through the atmosphere.

Given the site coordinates, we computed the modulation factor $\cos\theta_{\odot}$ as a function of day and local time. Local transit cosine values range between 1 around May 18 and July 28 (for 2008) and 0.74 at winter solstice (December 21). Knowing the position of the Sun at the site as a function of time, we can study the variable $\psi = F/(F_{\odot}\cos\theta_{\odot})$. The histogram of values of ψ is shown in Fig. 11. It has a bimodal distribution, with a first maximum at around $\psi \sim 0.2$ and a narrow peak at $\psi \sim 0.75$, with a minimum around 0.55. We interpret the narrow component as due to direct sunshine, while the broad component is originated when solar radiation is partially absorbed by clouds; we then use the relative ratio of these as the "clear weather fraction". Separating the data in intervals of $\cos\theta_{\odot}$, we observe that the minimum of the distribution of values of ψ increases with $\cos\theta_{\odot}$ for small airmasses to become constant at lower Solar elevations, following the empirical relation:

$$\psi_{min} = \begin{cases} 0.44\cos\theta_{\odot} + 0.195 & \text{for} \quad \cos\theta_{\odot} > 0.625\,, \\ 0.47 & \text{for} \quad \cos\theta_{\odot} \leqslant 0.625\,. \end{cases}$$

For this first analysis we separated data with $\psi \leqslant \psi_{min}$ as cloudy weather and data with $\psi > \psi_{min}$ as clear weather. We computed the fraction of clear weather (clear/clear+cloudy), for every hour of data. Only hours with at least 30 minutes of data were considered for the analysis, adding to 15223 hours of data. We considered data with airmasses lower than 10.

The median clear fraction for the site is 48.4%, consistent with values reported by Erasmus & Van Staden (2002). In a comprehensive study for the California Extremely Large Telescope (CELT) project, the authors surveyed cloud cover and water vapor conditions for different sites using observations from the International Satellite Cloud Climatology Project (ISCCP). The study period is of 58 months between July 1993 to December 1999 using a methodology that had

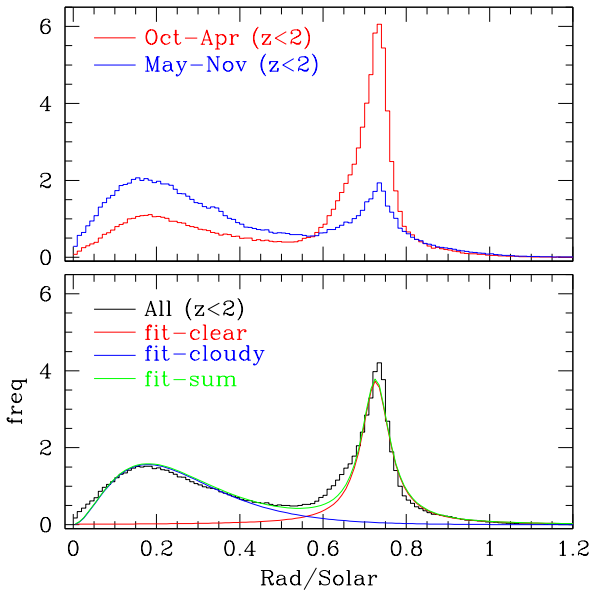

Figure 11. *Top:* the observed distribution of normalized solar fluxes for the wet and dry seasons. *Bottom*: the bimodal distribution of the solar flux divided by the nominal solar flux at the top of the atmosphere, $F_{\odot}\cos\theta_{\odot}(t)$. The distribution shows a bimodal behaviour which can be reproduced by a two component fit, show in solid lines. The relative area of both components determines the clear/cloud fraction. See the electronic edition of MNRAS for a color version of this figure.

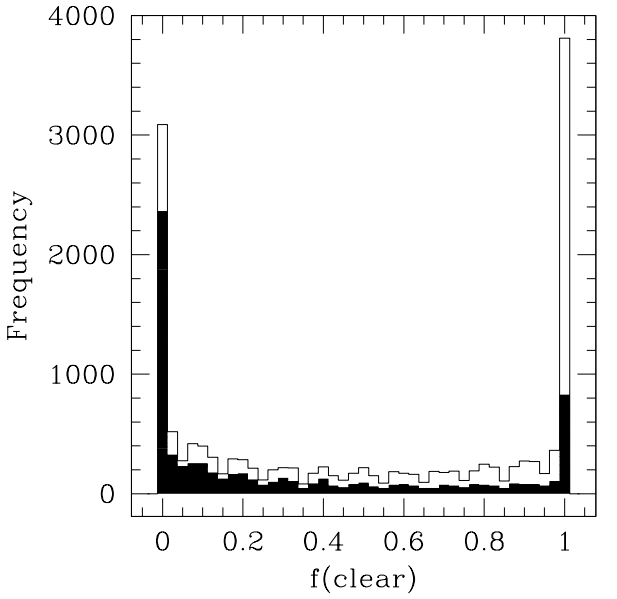

Figure 12. Distribution of hourly clear fraction for the 15223 datapoints available. The dark histogram shows the distribution for 7267 points of data taken in the (wet) months from May to October. The dry months are represented by the difference between both histograms.

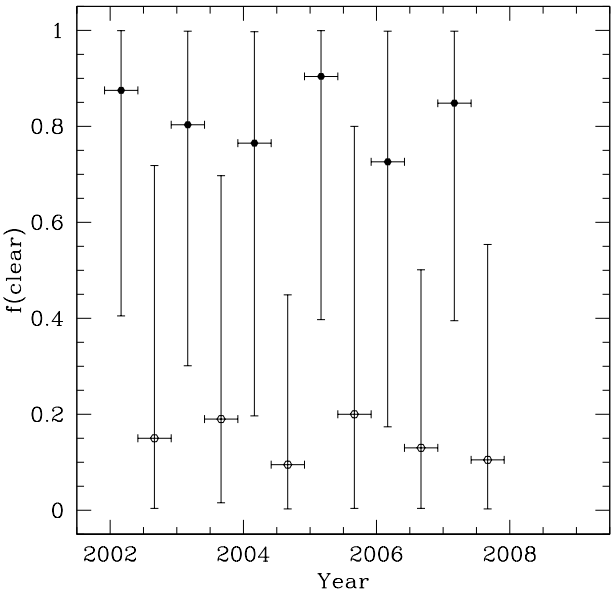

Figure 13. Graph showing clear fractions for the different season. Points are at median; bars go from 1st to 3rd quartile. Wet season (open dots) is the yearly interval from May to October; dry season (full dots) is from November to April of the following year.

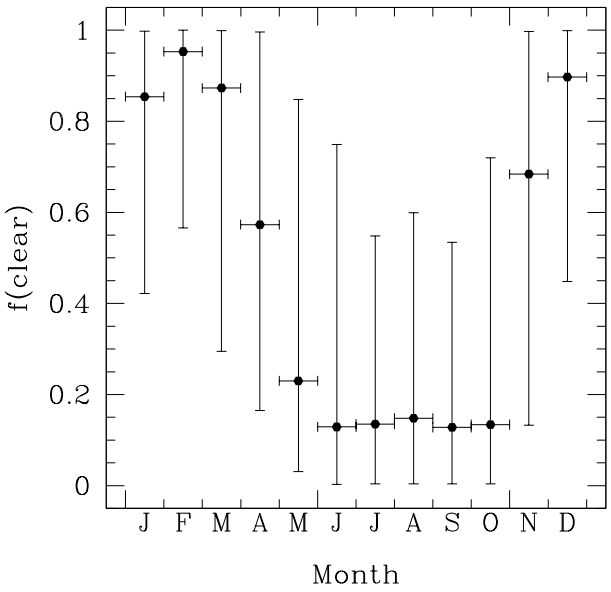

Figure 14. Graph showing the median and quartile values of the fraction of clear weather for the different months of the year.

been tested and successfully applied in previous studies. For Sierra Negra they measured a clear fraction for nighttime of 47%.

We note that the set of hourly clear fractions behaves in a rather bimodal fashion, as show in the histogram in Fig. 12: 20.3% of the hours have $f(\mathrm{clear}) = 0$, while 25.0% have $f(\mathrm{clear}) = 1$. The remaining (55%) have intermediate values. The histogram has a strong modulation in terms of wet and dry months. If we consider the semester between May and October the $f(\mathrm{clear}) = 0$ peak contains 32.5% of the data, while the $f(\mathrm{clear}) = 1$ has 11.4%. During the complementary dry months the $f(\mathrm{clear}) = 0$ peak contains 9.0% of the data, while the $f(\mathrm{clear}) = 1$ has 37.4%. Intermediate conditions prevail around 55% of the time in both semesters.

The contrast between dry and wet semesters is well illustrated in Fig. 13, showing the median and quartile fractions of clear time for successive wet and dry semesters. Semesters are taken continuously, from May to October representing the wet season and November to April of the following year for the dry season. The bars represent the dispersion in the data, measured by the interquartile range. Large fluctuations are observed at any time of the year. The contrast between the clearer dry months, with median daily clear fractions typically above 75%, and the cloudier wet months, with median clear fractions below 20%, is evident. The seasonal variation can be seen with more detail in the monthly distribution of the clear weather fraction, combining the data of different years for the same month, shown in Fig. 14. The skies are clear (f(clear)$>$ 80%) between December and March, fair in April and November (f(clear)$\sim$ 60%), and poor between May and October (f(clear)$<$ 30%). The fluctuations in the data are such that clear fractions above 55% can be found 25% of the time in the worst observing months.

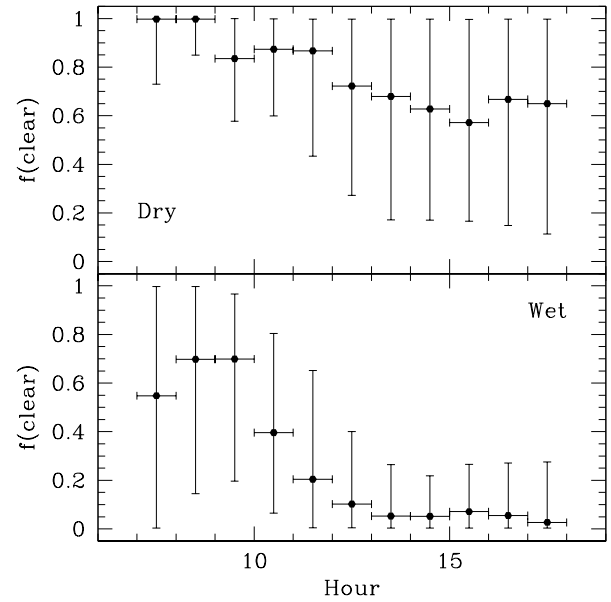

Figure 15. Graph showing the median and quartile values of the fraction of clear weather for each hour of day. The lower and upper are for wet (MJJASO) and dry (NDJFMA) semesters respectively.

Fig. 15 shows the median and quartile clear fractions as function of hour of day for the wet/dry subsets. The interquartile range practically covers the (0-1) interval at most times. We note that good conditions are more common in the mornings of the dry semesters, while the worst conditions prevail in the afternoon of the wet season, dominated by Monsoon rain storms. The trend in our results for daytime is consistent with that obtained by Erasmus and Van

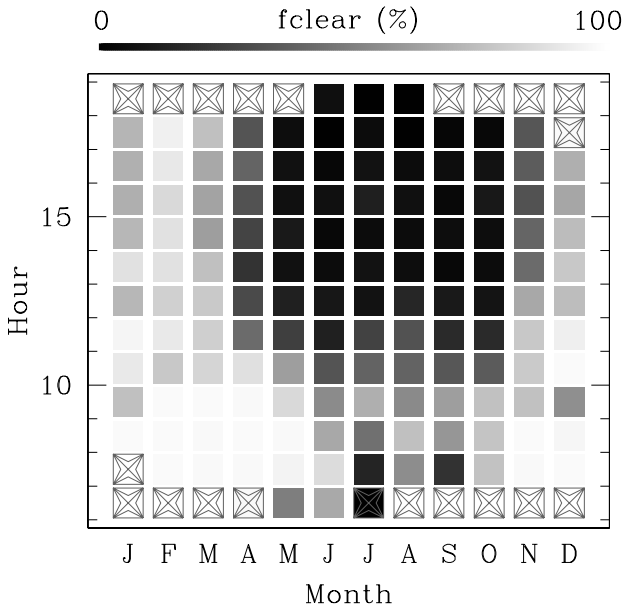

Figure 16. Grey level plot showing the median fraction of clear time for each month and hour of day. Squares are drawn when more than 10 hours of data are available; crosses indicate less than 30 hours of data.

Staden (2002). By analysing the clear fraction during day and nighttime they found that the clear fraction is highest before noon, has a minimum in the afternoon and increases during nighttime.

Fig. 16 shows a grey level plot of the median percentage of clear time for a given combination of month and hour of day. Dark squares show cloudy weather, clearly dominant in the afternoons of the rainy months (MJJASO). These are known to be the times of stormy weather in the near-equator. Clear conditions are present in the colder and drier months (NDJFMA). This plot is similar to that of humidity. In fact, when relative humidity decreases, the fraction of clear time increases. The relation between RH and f(clear) will be the subject of a forthcoming paper.

8 SUMMARY AND CONCLUSIONS

We have presented for the first time data and analysis of long-term meteorological data directly obtained from local meteorological stations at Sierra Negra. A comparison of the measurements from two weather stations was carried out by cross calibrating the data; to include the accuracy errors of both stations, we obtained a fit for each parameter by minimizing χ^2. In the case of the temperature the values of both stations are consistent. For the wind velocities the fit is not consistent wit the equality between the two data sets. However, we showed that their statistical behaviour is similar, probably the two stations are sampling the same wind but not simultaneously and the differences might be due to the topography of the site. We will present a more detailed analysis of the wind in a forthcoming paper. The relative humidity sensor of one of the station slides up with time providing data higher than the real ones. We verified our results with a third station and data from the NCEP/NCAR Reanalysis project database. In the case of atmospheric pressure and solar radiation we only have data from one of the stations. We reported the daily, seasonal and annual behaviour of temperature, atmospheric pressure, relative humidity, wind speed and solar radiation. The site presents a median temperature of 1.07 °C and an atmospheric pressure median of 590.11 mb. The results for these two parameters agree with a warm standard atmosphere model for which the base temperature would be $T_0 = 30.9$°C. As the site is influenced by the tropical storms moving off the Gulf of Mexico the median relative humidity has a strong seasonal dependence: while the median value for dry season is 50.92% for the wet season is 84.92%. The wind velocity median is 3.77 m s^{-1}, with a third quartile of 5.88 m s^{-1} and a maximum of 36.2 m s^{-1}; these values are below the three LMT specifications: to perform below 1 mm the wind speed must below 9 m s^{-1}; operation at any wavelength are stop if the wind velocity is 25 m s^{-1} and the design survival wind speed is 70 m s^{-1}. From the solar radiation data we developed a model for the radiation that allowed us to estimate the fraction of time when the sky is clear of clouds. The results obtained are consistent with Erasmus and Van Staden (2002) measurements of cloud cover using satellite data. This consistency shows the great potential of our method as cloud cover is a crucial parameter for astronomical characterization of any site. To our knowledge this is the first time that solar radiation data from the ground are used to estimate the temporal fraction of clear sky. The result presented here show that the meteorological conditions at Sierra Negra are stable daily and seasonally and have been so for the seven years measured. We consider that this period is representative of the climate at the site. Therefore Sierra Negra offers exceptional conditions for such a high altitude, specially during the dry season, and is an ideal site for millimeter and high energy observations.

ACKNOWLEDGEMENTS

NCEP Reanalysis data provided by the NOAA/OAR/ESRL PSD, Boulder, Colorado, USA, from their website at http://www.cdc.noaa.gov/. The authors thank G. Djordovsky, A. Walker, M. Schoeck and G. Sanders for their kind permission to use the results from the Erasmus and Van Staden (2002) report for Sierra Negra. Remy Avila and Esperanza Carrasco thanks CONACyT support through the grant No. 58291.

REFERENCES

Carrasco E., Carramiñana A., Avilés J. L., Yam O., 2003, PASP, 115, 879

Carrasco E., Avila R., Carramiñana A., 2005, PASP, 117, 104

Erasmus A., Van Staden C. A., 2002, "A satellite survey of cloud cover and water vapor in the western USA and Northen Mexico. A study conducted for the CELT project.", internal report

Höskuldsson, A., Robin, C., 1993, Bull. Volcanology 55, 571

Hughes D., 2008, Private communication

Kalnay E., et al., 1996, Bull. Amer. Meteor. Soc., 77, 437
Konopelko A., et al., 1999, Astrop. Phys., 10, 275.
Lindzen, R.S., 1979, Annual Review Planet Sci., 7, 199
Masciadri, E. & Egner, S., 2006, PASP, 118, 1604-1619
Press, F. & Siever, R. 1982, Earth, 3rd edition, W.H. Freeman & Co., San Francisco, CA.
Sarazin M., Tokovinin A., 2002, in Vernet E., Ragazzoni R., Esposito S., Hubin N., eds, ESO Conf. Workshop Proc. Vol.58, Beyond Conventional Adaptive Optics, ESO, Garching, Germany, p. 321
Rossotti, A. Ph.D. Thesis, Geociencias, UNAM (2005).

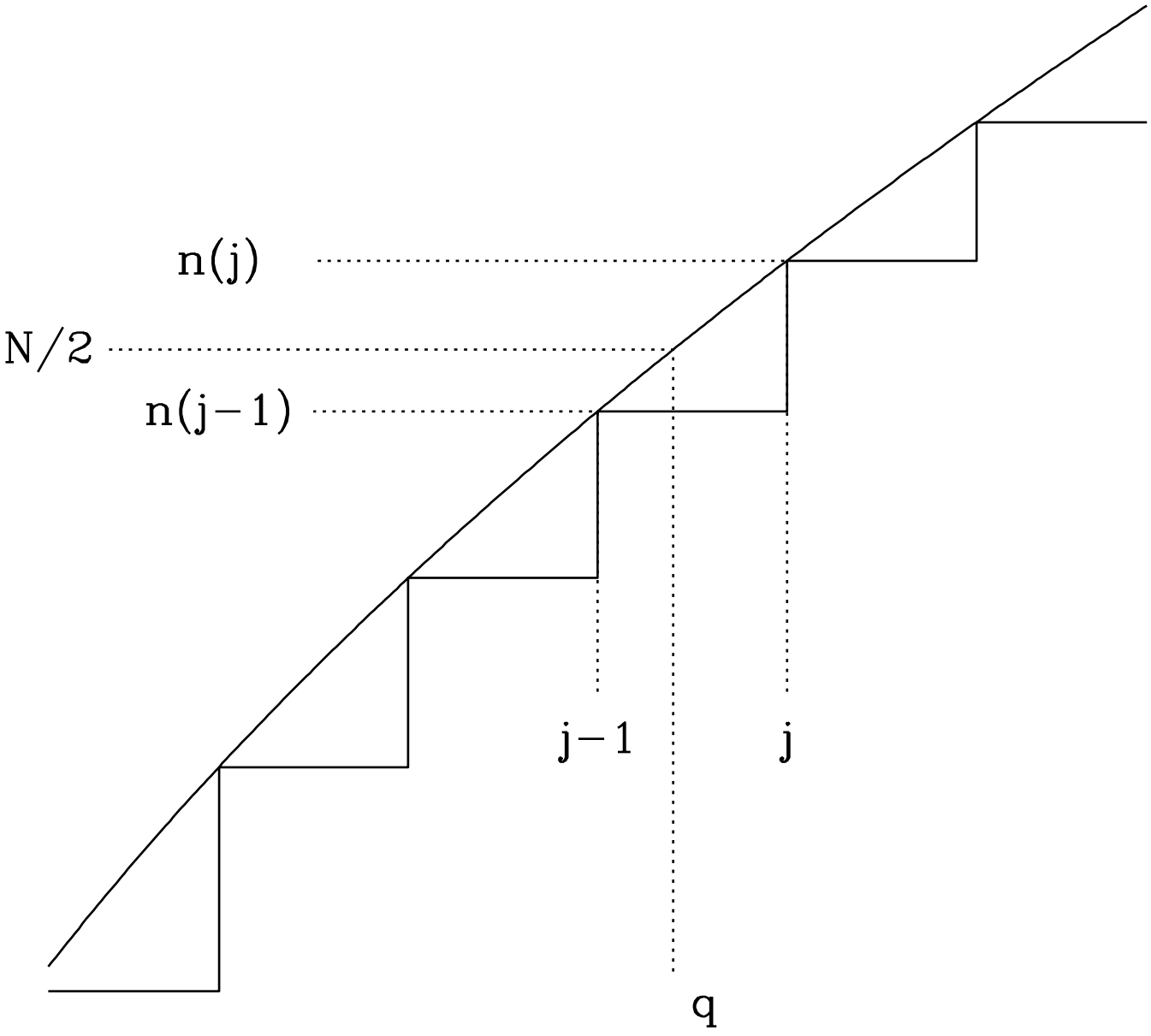
n(j)
N/2
n(j−1)
j−1
j
q